buildings

MDPI

Article

Ground Deformation of Shield Tunneling through Composite Strata in Coastal Areas

Xiong Wu [1], Jiangbo Xu [1,*], Shaowei Wang [1], Peng Sha [2,*], Zemin Han [1], Xinyu Chen [1], Sheng Shu [1], Wei Qiao [1] and Xianglong Zeng [1]

[1] School of Highway, Chang'an University, Xi'an 710064, China
[2] College of Civil Engineering, Shaoxing University, Shaoxing 312000, China
* Correspondence: xujiangbo@chd.edu.cn (J.X.); shapeng@usx.edu.cn (P.S.)

Abstract: In order to mitigate ground deformation during shield construction in both upper soft and lower hard strata of coastal areas, a numerical simulation was executed. This simulation assessed surface deformation under varying stratum ratios, grouting pressures, and earth bin pressures. The evaluation was primarily based on the amount of ground deformation, which revealed that hard rock strata offer superior settlement control compared to soft rock strata. The excavation of the right tunnel line increased disturbance to the left line at higher stratum ratios. Surface deformation demonstrated a linear correlation with earth pressure, with 130 kPa identified as the optimal point. Higher pressures resulted in extrusion deformation and ground uplift. Grouting pressure had a minimal impact on stratum deformation over time. The stratum ratio exerted the most significant influence on settlement, followed by earth pressure, with grouting pressure having the least impact. In the context of coastal tunnel construction, hard rock excavation is favored. Earth pressure must be balanced to prevent subsidence or uplift, while excessive grouting pressure does not significantly reduce subsidence. Grouting pressure should ensure the complete filling of voids.

Keywords: coastal areas; upper soft and lower hard strata; shield tunneling; construction parameters; ground deformation

check for updates

Citation: Wu, X.; Xu, J.; Wang, S.; Sha, P.; Han, Z.; Chen, X.; Shu, S.; Qiao, W.; Zeng, X. Ground Deformation of Shield Tunneling through Composite Strata in Coastal Areas. *Buildings* **2024**, *14*, 1236. https://doi.org/10.3390/buildings14051236

Academic Editor: Yong Tan

Received: 29 March 2024
Revised: 19 April 2024
Accepted: 24 April 2024
Published: 26 April 2024

Copyright: © 2024 by the authors. Licensee MDPI, Basel, Switzerland. This article is an open access article distributed under the terms and conditions of the Creative Commons Attribution (CC BY) license (https://creativecommons.org/licenses/by/4.0/).

1. Introduction

As urbanization progresses, subway construction has entered a phase of rapid expansion, with an exponential increase in newly constructed subway lines [1]. While urban subway construction technology is maturing, it still faces numerous engineering challenges due to complex geological conditions. Shield tunneling through soft upper hard lower strata represents one of the most intricate engineering problems. This process necessitates ensuring the safety and stability of the ground surface. If the surface subsidence is too large, cracks will inevitably occur, leading to surface collapse and causing road cracking, thereby resulting in huge economic and environmental losses [2–4]. Additionally, ground uplift can compromise the safety of ground-based buildings or structures. Consequently, it is of great significance to study the ground deformation caused by shield tunneling construction in the upper soft and lower hard strata of coastal areas.

The primary research methodologies for ground settlement induced by shield construction encompass empirical formula methods, mathematical analytical approaches, model testing techniques, field testing procedures, and numerical simulation methods. The empirical formula method originates from Peck's cross-sectional settlement formula for the ground surface under undrained conditions [5]. Subsequently, O'Reilly and New [6] elucidated the correlation between the settlement groove width coefficient and the tunnel center axis burial depth when the shield traverses either a single viscous land layer or a non-viscous land layer. Mair et al. [7] further generalized Peck's theory to more profound scenarios. Attewell et al. [8] advocated for the utilization of cumulative probability curve

formulas to compute longitudinal ground surface settlement groove curves above the tunnel axis. Liu and Hou [9] initially introduced the concept of "underground loss" based on Peck's formula method, subsequently revising the Peck calculation formula to estimate predicted ground surface longitudinal settlement. Subsequent scholars expanded this approach to accommodate double-line tunnel longitudinal settlement calculations [10,11]. A multitude of researchers have employed the empirical formula method in their studies, notably including the mirror method, the stress function method in polar coordinates [12], the complex variable function method [13], the random medium theory [14], the energy conservation method, and the deformation prediction method grounded in Mindlin's basic solution [15]. Drawing upon similar theoretical frameworks, He et al. [16] conducted indoor model tests to investigate the ground deformation settlement induced by tunnel excavation. He et al. [17] employed field engineering data to analyze the disturbance patterns of adjacent strata using a force shield. In light of advancements in computer technology, researchers have utilized discrete element analysis software [18], boundary element software [19], finite element software [20], and finite difference software [21] to assess the impact of shield construction on ground settlement. The research methods can be summarized in chronological order as shown in Table 1.

Table 1. Research methods.

Method	Research Result	Author	Year
Empirical formula methods	Cross-sectional settlement formula	Peck [5]	1969
Empirical formula methods	The correlation between settlement groove width coefficient and tunnel center axis burial depth	O'Reilly and New [6]	1982
Empirical formula methods	Vertical surface settlement trough curve	Attewell et al. [8]	1986
Empirical formula methods	Vertical surface settlement trough curve	Liu and Hou [9]	1991
Mathematical analytical methods	Mindlin's basic solution	Rowe and Lee [15]	1992
Empirical formula methods	Calculation of lateral settlement of deep soil	Mair et al. [7]	1993
Field testing procedures	Field test	He et al. [17]	2012
Model testing techniques	Indoor model tests	He et al. [16]	2013
Mathematical analytical methods	Random medium theory	Zeng et al. [14]	2016
Mathematical analytical methods	Complex variable function method	Zhang et al. [12]	2017
Mathematical analytical methods	Mirror method	Yuan et al. [22]	2018
Mathematical analytical methods	Stress function method in polar coordinates	Kong et al. [13]	2019
Numerical simulation methods	Boundary element method	Yang et al. [19]	2019
Empirical formula methods	Settlement of double-track shield tunnel	Zhang et al. [11]	2021
Numerical simulation methods	Finite difference method	Li et al. [21]	2022
Numerical simulation methods	Discrete element method	Feng et al. [18]	2023
Numerical simulation methods	Finite element method	Lei et al. [20]	2024

Numerous factors influence shield construction, a topic that has been extensively researched by scholars. Guo [23] examined the impact of tunnel burial depth, overlying stratum conditions, and stratum conditions at the tunnel borehole on ground settlement. It is found that surface subsidence is significantly influenced by the conditions of the overlying strata and is closely related to the properties of the strata close to the surface. Zhou et al. [24] investigated the relationship between ground settlement and varying soft–hard composite ratios of strata. It is found that there is a significant difference in surface subsidence between different composite heights of soft and hard rocks compared to strata. Ochmanski and Modoni [25] analyzed the sensitivity of two influencing factors of grouting pressure and grouting parameters to ground settlement deformation. The outcomes of the analysis highlight the three-dimensional nature of the deformation mechanisms taking place near the advancing front, the effects produced by the different tunnelling operations, and the role of the different structural elements. Anato et al. [26] explored the effects of tunnel lining strength, grouting strength, and shield excavation speed in heterogeneous soils on ground settlement.

Researchers have conducted extensive studies on ground subsidence using various methodologies, identifying the primary factors influencing this phenomenon. However, the empirical formula method lacks robust theoretical backing, and the numerical analytical approach for residential rows requires enhancement. While model tests offer relative accuracy, they are time-consuming and costly. Field testing methods are constrained by site conditions and construction timelines. Numerical simulation methods, on the other hand, amalgamate the strengths of these research techniques and have garnered official recognition. Although numerous factors associated with shield construction contribute to ground subsidence, the systematic study and analysis of three key determinants—stratum composite ratio, grouting pressure, and earth bin pressure—are lacking. This paper addresses the ground deformation resulting from shield construction parameters in upper soft and lower hard strata. Utilizing the finite difference software, combined with the modeling feasibility machine calculation efficiency of numerical simulation, we simulate and analyze the impact of these three parameters on ground deformation. Surface settlement serves as our evaluation metric to discern the sensitivity of each factor.

2. Project Overview

Qingdao is a beautiful coastal city located in the eastern coastal area of China. Shield tunneling technology has played a crucial role in the construction of the subway in Qingdao [27]. The geological characteristics of Qingdao, characterized by upper soft and lower hard strata, pose unique challenges to shield tunneling construction (see Figure 1). Overcoming the difficulties of shield tunneling construction in upper soft and lower hard strata can ensure the safety and quality of subway tunnel construction. Therefore, this study utilizes a double-line shield section of the Qingdao Metro, featuring a tunnel diameter of 6.0 m. The left-line tunnel measures 1112.485 m in length, while the right-line tunnel extends to 1114.920 m. The arch top burial depth ranges between 7.0 m and 17.2 m. The tunnel primarily traverses strata such as silty clay, medium-coarse sand, pebble soil, strongly weathered granite, and slightly weathered granite. The left line passes through the upper soft lower hard stratum for approximately 333 m, while the right line does so for about 271 m. This segment is classified as having a risk level II.

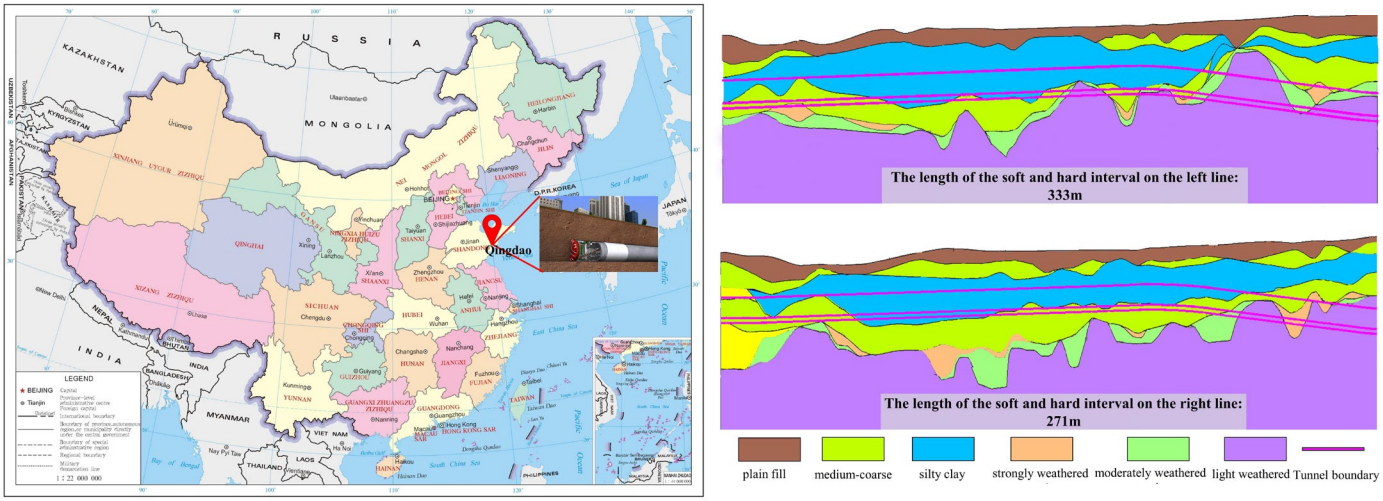

(**a**) (**b**)

Figure 1. Engineering location and geological conditions: (**a**) location of the project and (**b**) interval tunnel longitudinal cross-section.

3. Methodology

The finite difference method is a numerical solution, whose basic idea is to first mesh the domain of the problem, and then replace the derivative in the definite solution problem with the difference at the grid points using appropriate numerical differentiation formulas,

thereby discretizing the original problem into a difference format and obtaining a numerical solution. The finite difference method has the characteristics of simplicity, flexibility, and strong universality, making it easy to implement on computers. This study employs numerical simulation software, grounded in the finite difference method, to meticulously simulate and scrutinize the deformation law of strata under varying shield construction parameters. The process can be delineated into several detailed steps:

3.1. Numerical Model Establishment

(1) Model simplification and basic assumptions

The geological conditions within the upper soft and lower hard composite strata of the research interval are both complex and variable. Furthermore, the construction of the double-line tunnel occurs asynchronously within this interval. If a simulation is predicated on these actual geological and construction conditions, it results in a high degree of difficulty in model establishment and low calculation efficiency. To address this, we must consider the engineering realities of the interval and our primary research objectives, while ensuring accuracy in our research. This necessitates the simplification of our numerical calculation model. The following basic assumptions are made to simplify this model:

① In order to accurately represent the characteristics of both the upper soft and lower hard strata, a comprehensive study is undertaken. It is postulated that the model strata are segmented into three distinct layers: the overlying soil layer, the shield tunneling layer, and the overlying foundation rock layer. These strata are subsequently simplified to a horizontal layered distribution to improve computational efficiency.

② The influence of transient disturbances, such as the duration of grouting solidification on surface settlement, is not taken into account. These disturbances exhibit significant randomness and short-term action time, yet they exert a relatively minor effect on the ultimate distribution of surface settlement.

③ The deformation caused by the decrease in the breaking strength of the rock and soil structure around the tunnel is not considered due to the friction of the shield shell and the disturbance of the cutter head of the excavation face to the rock and soil mass. There is a gap between the actual excavation tunnel and the shield shell, and the friction disturbance to the surrounding rock and soil can be ignored.

④ The grouting effect of shield tail and the ground loss caused by shield over-excavation are simplified into homogeneous elastic equivalent layers with equal thickness.

(2) The Dimensionality of the Model and Boundary Conditions

The numerical model is modeled by the native method of finite difference software and modeled by command flow. The model under consideration focuses on the shield tunnel and its adjacent rock mass, utilizing geometric models constructed through radical-cylinder, cylinder, cylindrical-shell, and brick methodologies. The tunnel is situated 7 m below ground level, with a diameter of 6.2 m during excavation. In accordance with the Saint-Venant's principle, the impact range of the shield tunnel's advancement on the surrounding strata approximates 3–5 times the tunnel's diameter. Considering real-world conditions, the model's width is designated as 84.4 m and height as 46.2 m, and the length of the heading direction is an integer multiple of the number of heading rings, which is set to 120 m. Consequently, a calculation model with length × width × height of 120 m × 84.4 m × 46.2 m is obtained, as shown in Figure 2. The maximum length of the grid is 2 m, and the key area adopts a more refined grid size, a total of 563,200 grids, so that the calculation efficiency of the model can be guaranteed, and the deformation of the key area can be considered in detail. The model design of shield tunnels such as tunnels, grouting layers, and segments is shown in Figure 3.

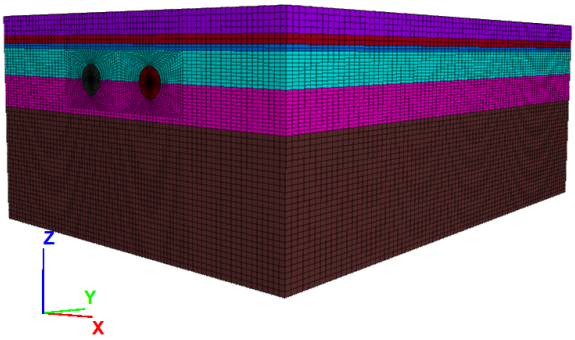

Figure 2. Three-dimensional numerical model.

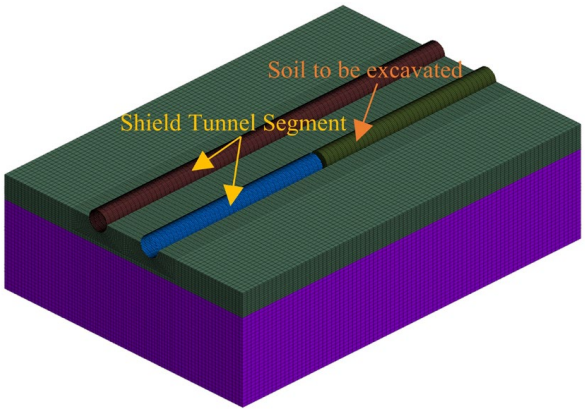

Figure 3. Design of shield tunnel structure model.

The boundary condition of the model is set as follows: two interfaces in the *X*-direction impose an *X*-displacement constraint, while two interfaces in the *Y*-direction apply a *Y*-displacement constraint. The displacement constraint in the *Z*-direction is applied to the bottom interface of the model. Conversely, the top surface of the model functions as a free interface, as illustrated in Figure 4.

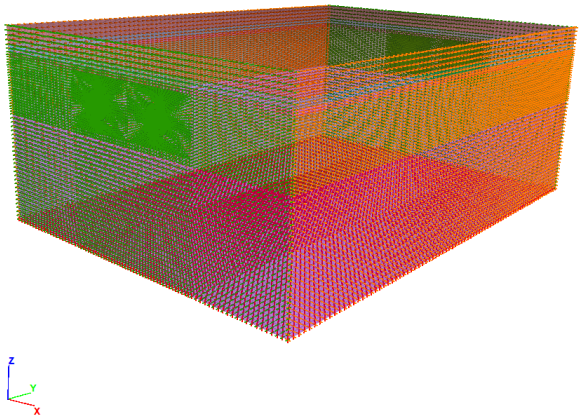

Figure 4. Setting of boundary conditions.

(3) Model calculation parameters

The rock–soil body surrounding the shield tunnel experiences elastoplastic deformation. The Mohr–Coulomb constitutive model is utilized to select the rock–soil body, while the elastic model is employed for the grouting layer. Additionally, the pipe segment adopts a shell structure unit. By analyzing the geological survey report of the section, typical physical mechanical parameters of the shield, which traverse upper soft and lower hard strata, are converted to obtain the model's physical parameters. These parameters are presented in Table 2.

Table 2. Formation parameters.

Strata	Density ρ/(kg·m^{-3})	Bulk Modulus K/MPa	Shear Modulus G/MPa	c/kPa	φ/°
Plain fill soil	1800	22	7	19.2	18
Fine sand	1750	29	13	0	22
Silty clay	1970	25	9	23	20
Coarse gravel sand	2050	41	21	80	35
Strongly weathered granite	2300	49	33	170	38
Moderately weathered granite	2500	8621	6198	500	40
Slightly weathered granite	2650	17,778	13,333	2000	45
Slurry	2100	56.2	38.7	—	—
Segments	2500	7000	4200	—	—

3.2. Shield Construction Simulation

(1) Simulation implementation of shield tunneling process

The tunnel diameter of the model is 6.2 m, and each cut's excavation length equals 1.5 m, which corresponds to a ring pipe slice width. The left and right double-line tunnels are both 120 m in length, necessitating 160 cycles of excavation for each working condition. The process of excavation is depicted in Figure 4. The earth bin pressure is achieved by applying pressure perpendicular to the face. After each ring's excavation, grouting is performed on the preceding ring. This grouting layer is modeled using an equivalent layer with a thickness of 0.1 m. The grouting pressure is achieved by applying a surface force perpendicular to the surrounding rock. The pipe slices are modeled using isotropic shell structure units. A comprehensive representation of the shield tunneling process can be found in Figure 5.

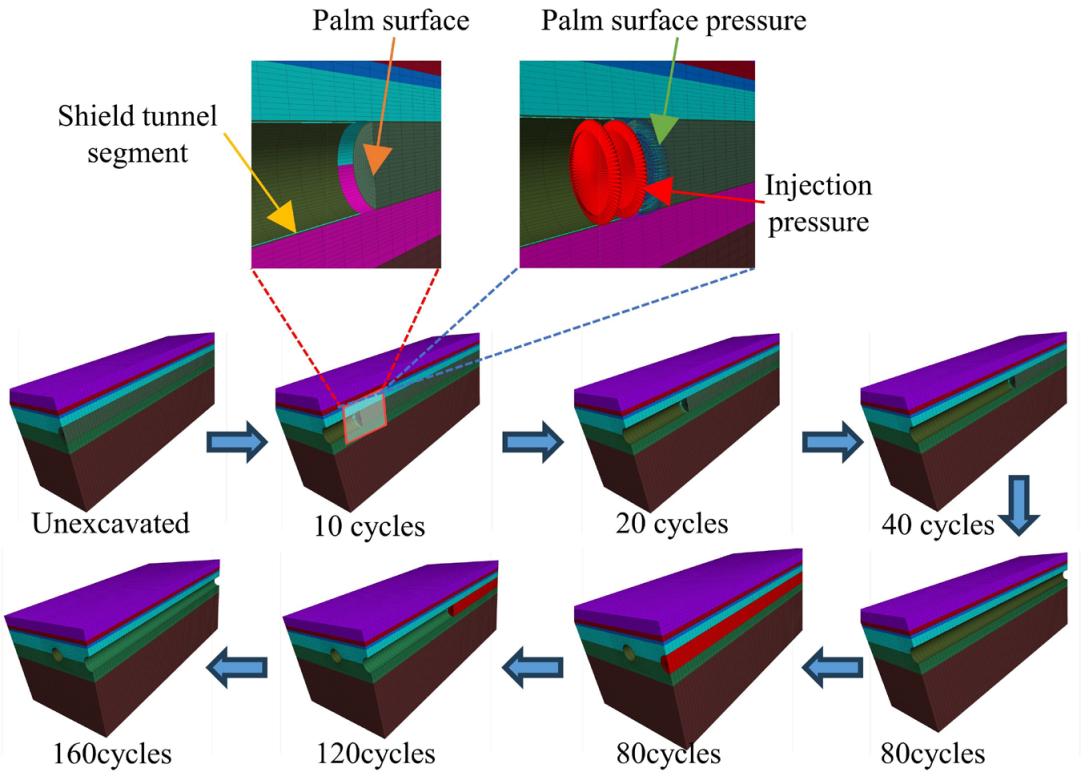

Figure 5. Shield excavation process.

(2) Numerical simulation scheme

In the construction process, excavation of the left-line tunnel commences before that of the right-line tunnel. To evaluate the influence of various construction parameters on stratum deformation, specific variables such as the stratum composite ratio, soil bin pressure, and grouting pressure are selected for simulation analysis. The engineering design of construction parameters delineates specific working conditions, as detailed in Table 3. The numerical simulation recommends an excavation length per step of 1.5 m, consistent with actual construction practices. Throughout the simulation, both displacement changes along and perpendicular to the tunnel axis are meticulously recorded and analyzed.

Table 3. Numerical simulation conditions.

Condition	1	2	3	4	5	6	7
Composite ratio (%)	0%	20%	40%	50%	60%	80%	100%
Soil pressure (kPa)	100	120	140	160	180	200	-
Grouting pressure (kPa)	200	250	300	350	400	-	-

4. Results

Variations in construction parameters can result in significant disparities in the geological patterns and deformation observed within shield tunnels. The outcomes of numerical simulations for each operational condition are detailed below:

4.1. Deformation in Formation under Various Composite Strata Ratios

The geological conditions play a pivotal role in determining the surface settlement of shield tunneling through both soft and hard strata within the section, primarily due to the interplay between these strata on the excavation surface. Figure 6 delineates the specific distribution of this model. The ratio of soft to hard rocks exhibits variability within the third and fourth soil layers. In the lower layer, characterized by a pronounced weathered granite fracture zone, its strength and other physical and mechanical attributes are susceptible to reduction. To refine the accuracy of numerical simulations, this study integrates the existing research findings and minimizes the rock parameters of the weathered fracture zone. The developed model is subsequently computed and scrutinized in this section.

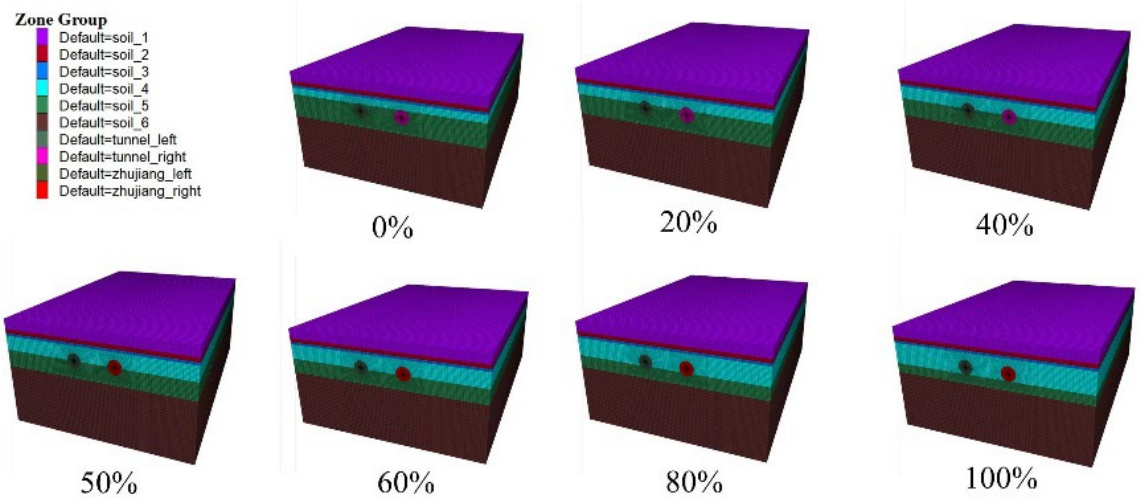

Figure 6. Soft–hard rock layer combination ratio numerical model diagram.

The strata's settlement demonstrates diverse laws of variation as excavation progresses. Following 80 cycles of excavation, the left-line tunnel is successfully traversed. Figure 7 illustrates the final settlement cloud map for strata with varying composite ratios. In contrast, the right-line tunnel begins at cycle 81, and after 160 cycles, it is also successfully

traversed. The final settlement cloud map for strata with different composite ratios is depicted in Figure 8 upon the completion of the right-line excavation. Figure 9 displays the settlement cloud diagrams at a Y = 60 m cross-section under seven distinct stratum composite ratios, corresponding to the completion of excavation in both the left- and right-line tunnels. Figure 10 illustrates the ground surface deformation under different stratum composite ratios.

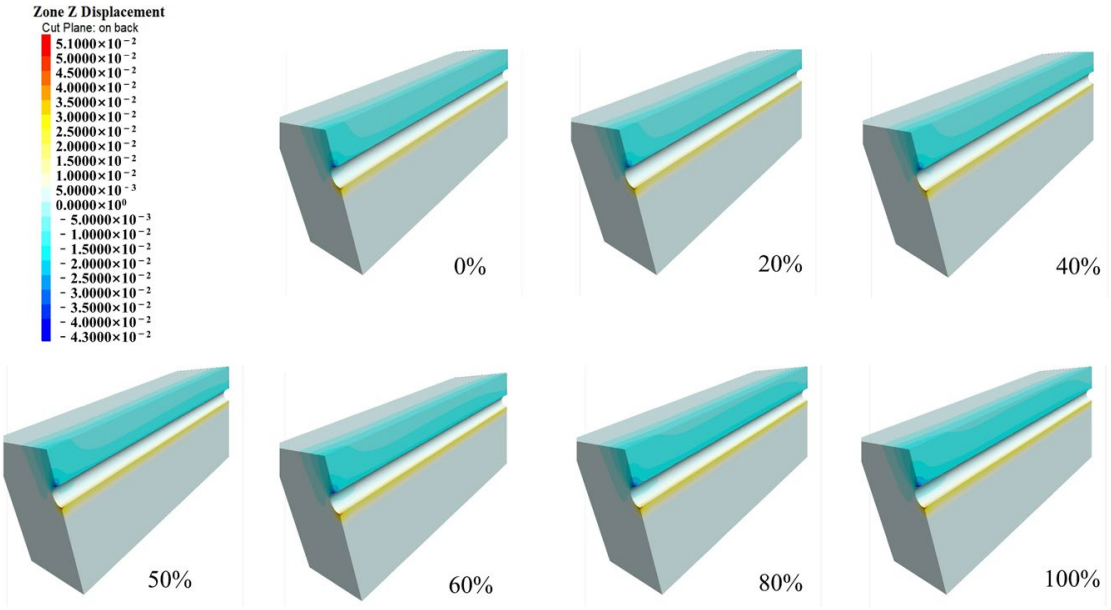

Figure 7. Cloud map of different composite ratio strata settlements after left-line excavation is completed.

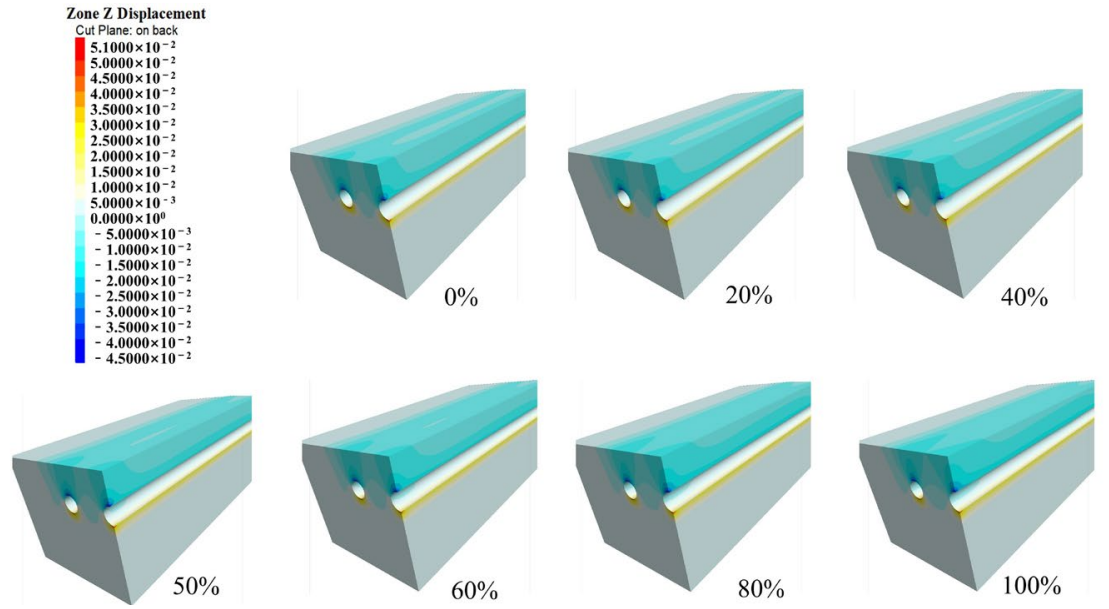

Figure 8. Strata settlement cloud diagram after completion of right-line excavation.

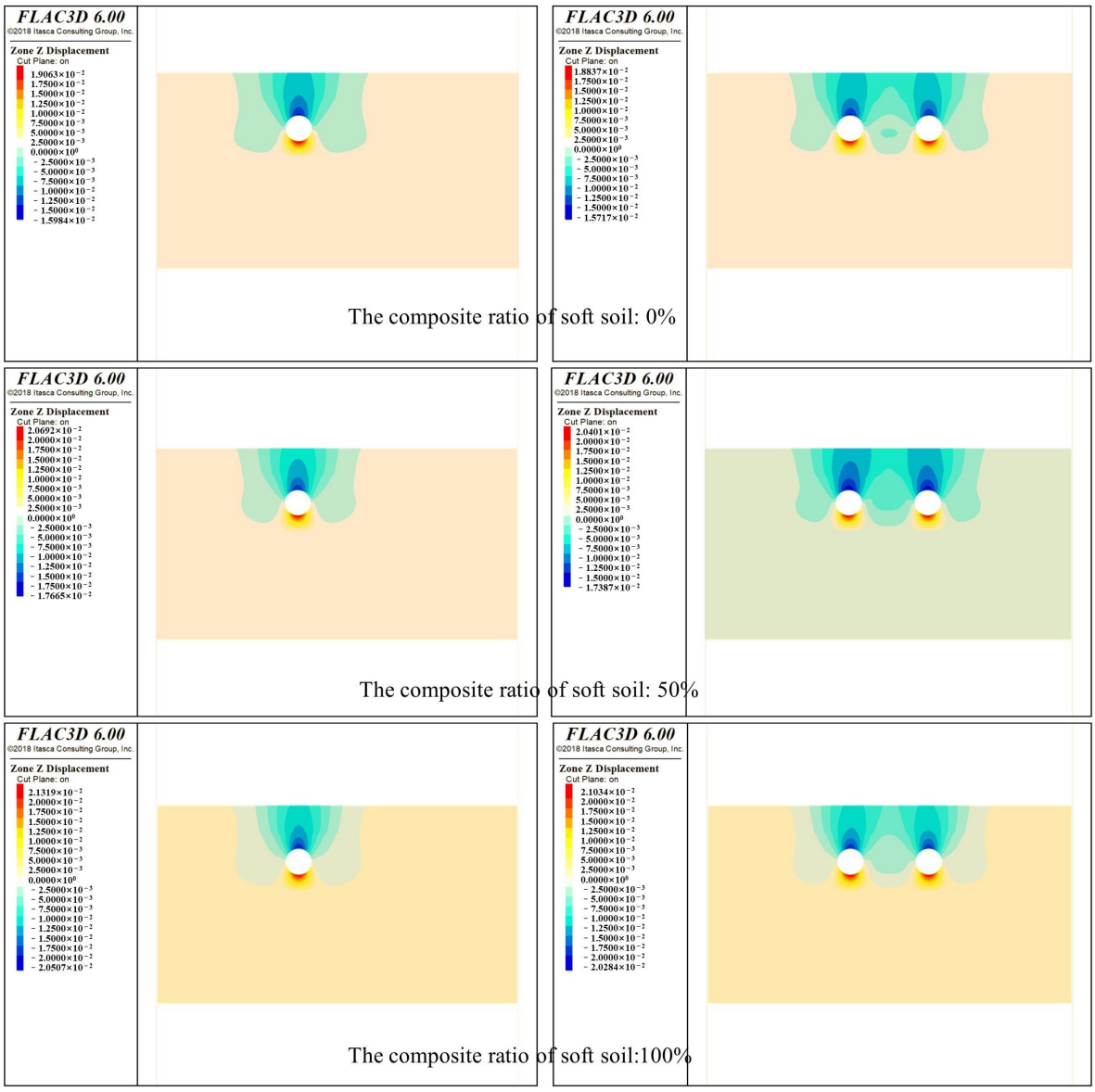

Figure 9. Sedimentation cloud map at Y = 60 m cross-section under different stratum composite ratios.

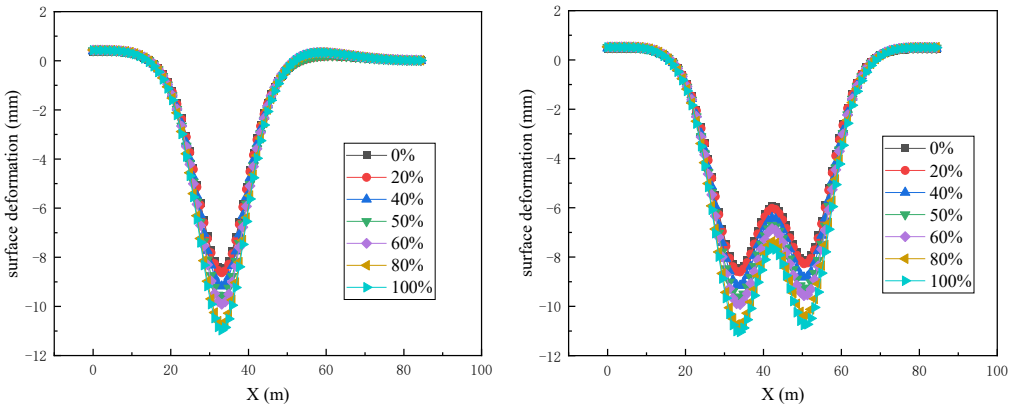

(**a**) (**b**)

Figure 10. Surface deformation curves under different stratum composite ratios: (**a**) left-line tunnel boring completion and (**b**) right-line tunnel boring completion.

Figure 11 illustrates the settlement curves of double-line tunnels under different stratum composite ratios. Figure 12 illustrates the variation in the settlement amount of the left-line tunnel.

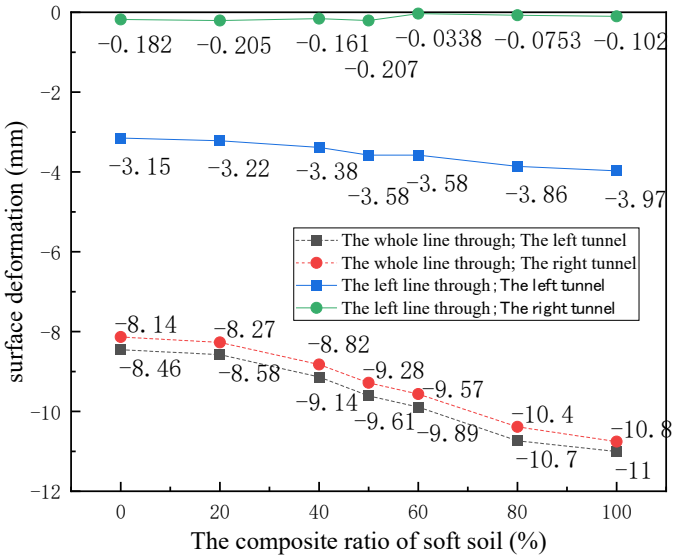

Figure 11. Settlement curves of double-track tunnels under different strata composite ratios.

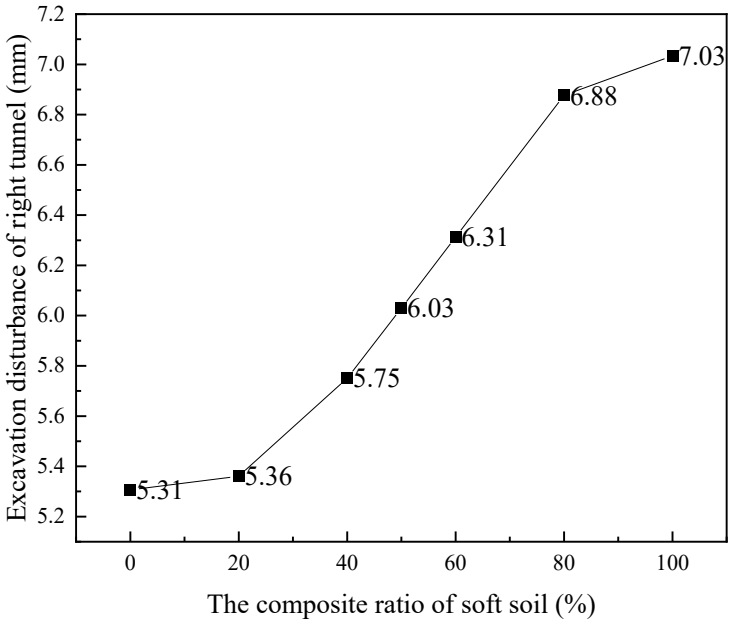

Figure 12. Excavation disturbance of right-line tunnel under different strata composite ratios.

The subsidence resulting from the excavation of double-line tunnels demonstrates a superimposition effect, with this phenomenon being most noticeable in the central region of the joint line between the two tunnel axes. Figure 13 depicts the trend of settlement value changes at various construction stages in relation to variations in the stratum composite ratio.

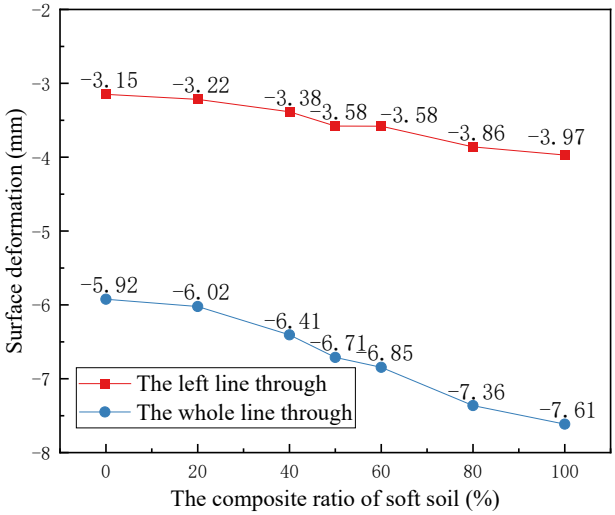

Figure 13. The variation curves of settlement values at the axis section in tunnels with different construction stages as a function of formation composite ratio.

4.2. Deformation in Formation under Different Soil Bin Pressures

In the auger chamber, if the earth pressure surpasses both the static earth pressure at the excavation face's center and the passive earth pressure of the excavation face, the excavation face becomes unstable and may be destroyed. This can lead to an uplift deformation of the surface. Conversely, when the earth pressure falls below the active earth pressure, the excavation face also experiences instability and potential destruction, resulting in the significant subsidence deformation of the surface. Consequently, maintaining the stability of the excavation face is crucial by controlling the size of the earth pressure chamber. In this study, we investigate the effects of various earth pressure chamber boring modes on surface subsidence. Using actual construction parameters, we examine six distinct earth pressure chambers and their impact on surface subsidence. We then simulate numerical calculations for 100 kPa, 120 kPa, 140 kPa, 160 kPa, 180 kPa, and 200 kPa to generate a longitudinal displacement cloud diagram of strata under different earth pressure chambers, as depicted in Figure 14.

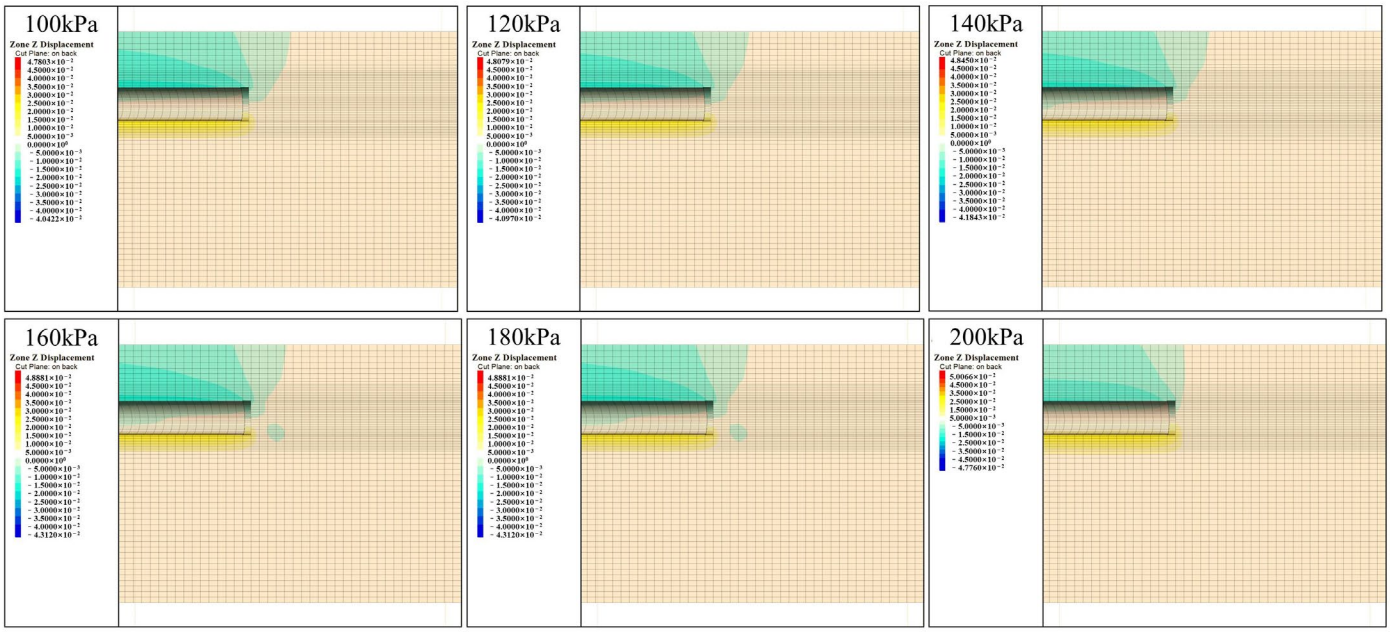

Figure 14. Stratigraphic longitudinal displacement cloud map under different soil bin pressures.

In the monitoring section with a length of 60 m (Y = 60 m), the distribution of surface lateral displacement at the shield's arrival time and the variation in the maximum value of surface settlement relative to soil bin pressure are depicted in Figures 15 and 16, respectively.

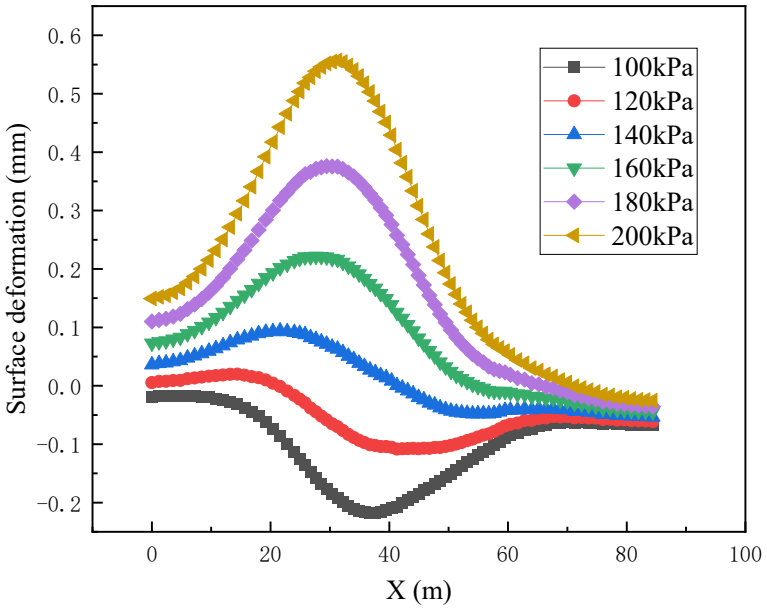

Figure 15. The surface settlement curve under different soil pressures when the shield arrives.

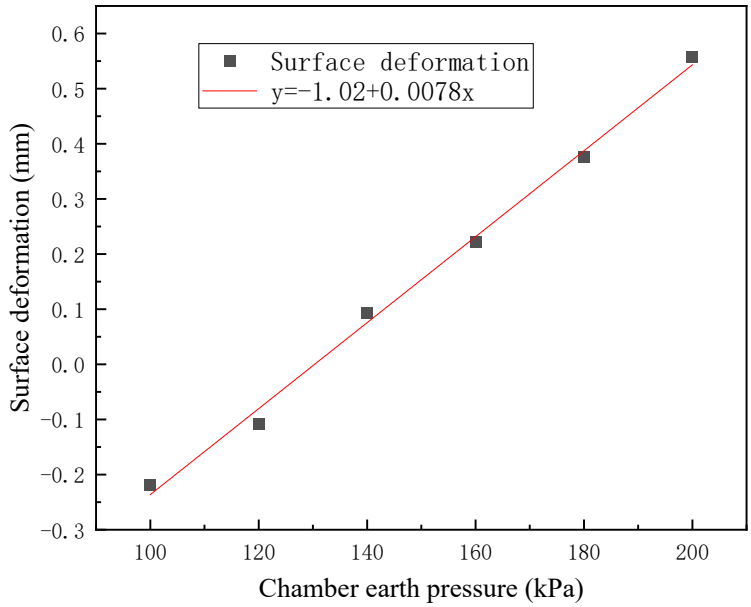

Figure 16. The variation curve of the maximum deformation of the ground surface with the earth pressure when the shield arrives.

4.3. Deformation in Formation under Different Grouting Pressures

In shield construction, the determination of grouting pressure is pivotal. Excessive pressure can result in slurry breaching the shield tail seal, leading to its flow towards the excavation face or earth pressure bin. Conversely, a lower pressure may leave an insufficient slurry filling at the top pipe segment, causing it to float upwards and become uneven, thereby leading to significant ground surface subsidence. To ensure complete slurry filling in the shield tail voids, it is imperative that the grouting pressure does not fall below the water–soil pressure of the stratum. To counteract surface deformation and damage induced by excessive grouting pressure, it is customary to employ 1.1~1.2 times

the static earth pressure. In this study, we examined five working conditions with grouting pressures of 200 kPa, 250 kPa, 300 kPa, 350 kPa, and 400 kPa to assess the influence of grouting pressure on ground surface subsidence through numerical simulation. The resulting ground settlement cloud diagrams under these varying grouting pressures are depicted in Figures 17 and 18.

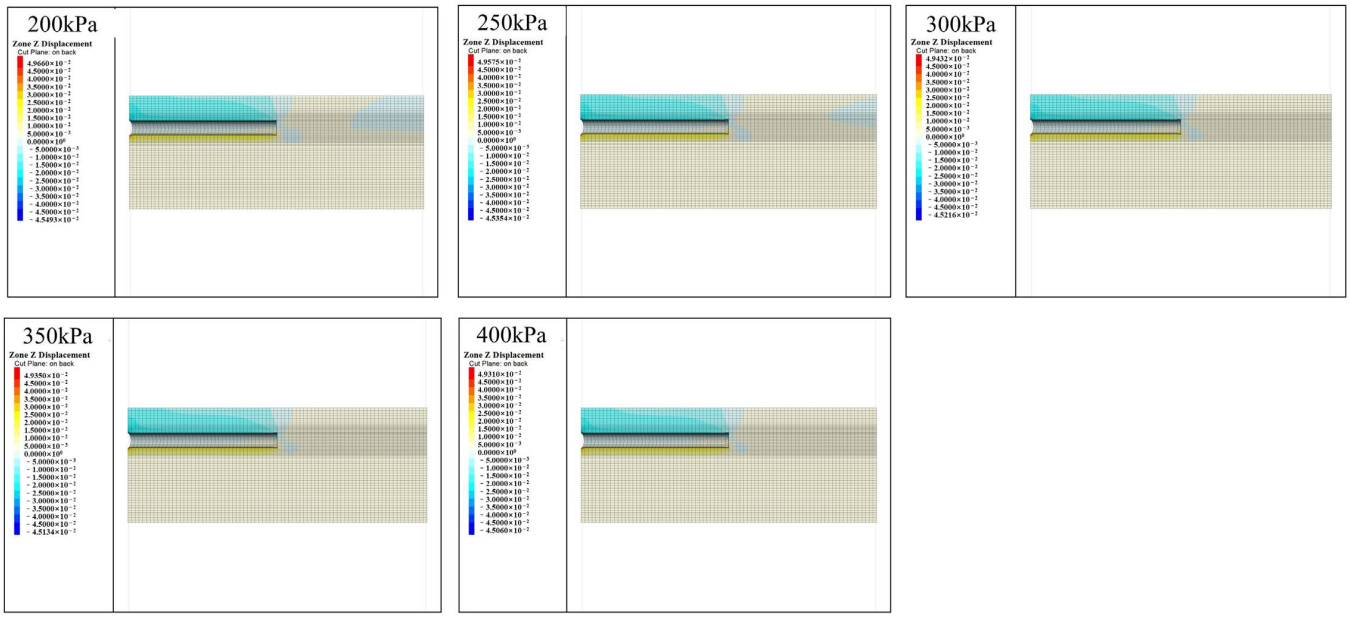

Figure 17. Cloud map of longitudinal settlement of formation under different grouting pressures.

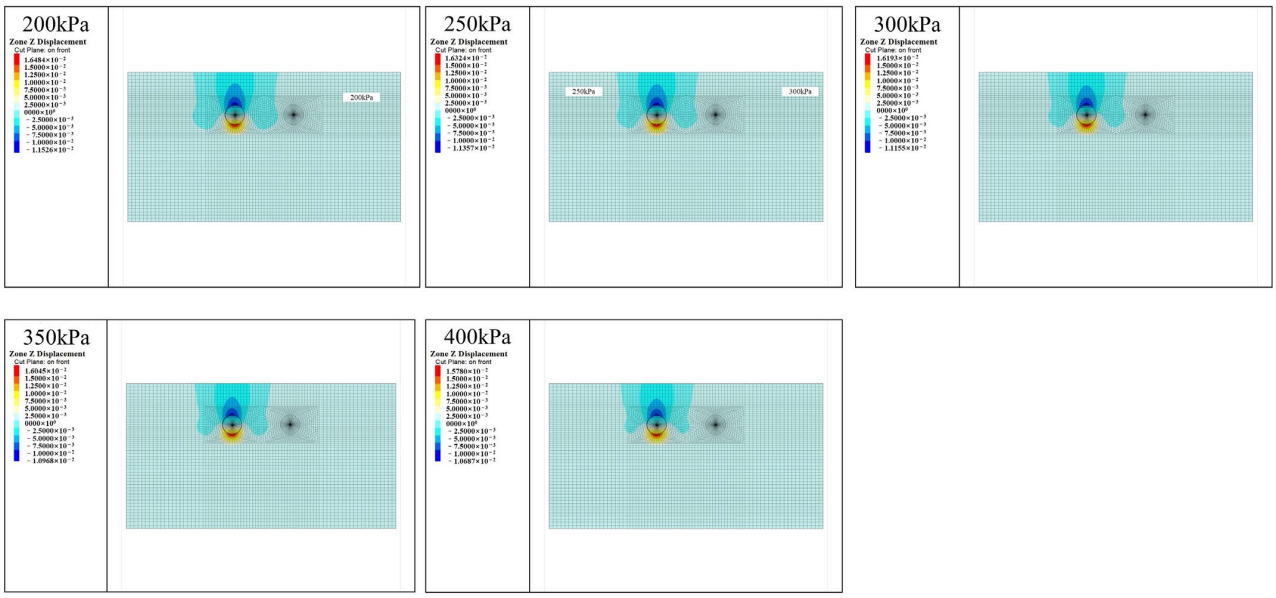

Figure 18. Cross-section settlement cloud diagram of strata under different grouting pressures.

The influence of lateral settlement curves on the surface under grouting pressure is illustrated in Figure 19. These figures represent the surface settlement at Y = 58.5 m, where the shield machine has been excavated to Y = 60 m. Considering that the grouting phase lags behind the shield excavation by one ring, Y = 58.5 m is chosen as the monitoring face. Figure 19a illustrates the surface settlement curve upon the arrival of the shield, while Figure 19b displays the surface settlement curve when the left line passes through.

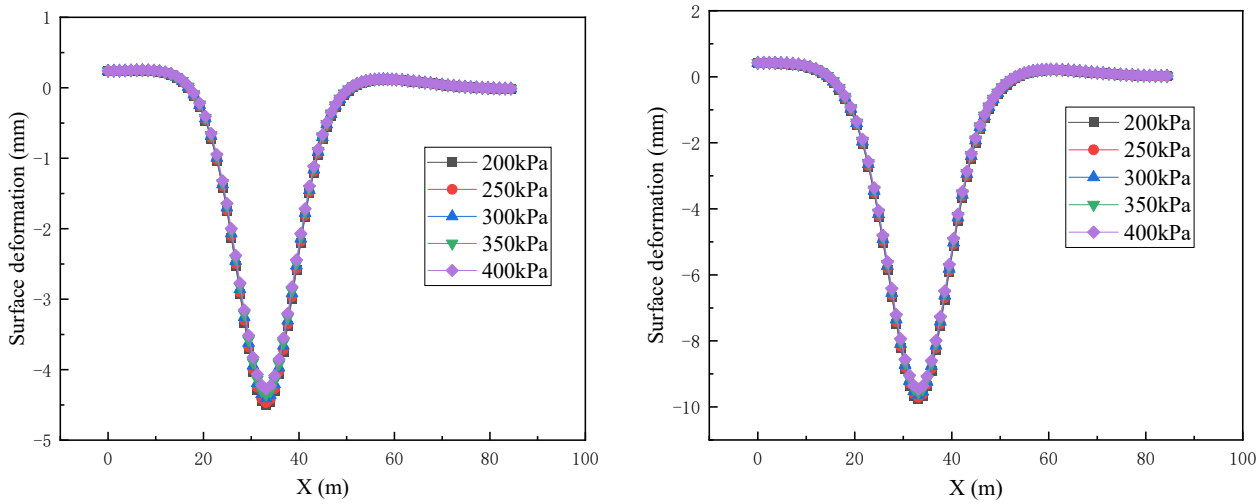

Figure 19. Lateral surface settlement under the influence of grouting pressure: (**a**) the shield arrival and (**b**) the left line passes through.

5. Discussion

5.1. Effect of Composite Strata Ratios on Settlement

As depicted in Figures 7 and 8, the variation in the combination ratio of soft and hard strata can result in significant differences in stratum settlement. Typically, the settlement pattern of strata demonstrates high consistency, with settlement occurring at the tunnel arch's apex and uplift at its base. Additionally, the temporal variation patterns of different composite ratio strata settlements are largely consistent, with both left-line and right-line tunnels exhibiting similar distribution laws. It is clear that the shield settlement time course curve exhibits minimal sensitivity to stratum composite ratios. The primary distinction among each settlement cloud diagram is the maximum settlement values. To further investigate the settlement induced by varying stratum composite ratios, a lateral section settlement at Y = 60 m within the model was selected for examination. Upon analysis of the displacement cloud diagram, it is evident that the shield construction displays unique characteristics in relation to both the tunnel's surrounding rock and surface displacement. These characteristics are contingent upon the variation in stratum composite ratios.

The settlement induced by the tunnel shield primarily manifests as a subsidence in the top area of the tunnel soil, while an increase in uplift displacement is observed in the bottom soil due to continuous excavation. This phenomenon can be attributed to the tunneling construction of the shield machine, which affects the surrounding rock strata. Consequently, there is a tendency for the strata to shrink towards the tunnel's interior. Additionally, a phenomenon known as unloading rebound occurs post-excavation at the tunnel's base, leading to the settlement of the arch roof and the upliftment of the tunnel floor slab [28].

In instances where the left-line tunnel is constructed first, it disrupts the original stress equilibrium of the soil body and induces disturbances within the stratum. Subsequently, when a right-line tunnel is constructed later, it triggers secondary disturbances to the soil body. The impact of these disturbances becomes compounded, leading to increased stratum deformation. Notably, this disturbance escalates with an increase in the stratum composite ratio. Generally, the influence of excavation soil on both the soil body and surface begins at the midpoint between the two tunnels, exhibiting a trend towards three-dimensional diffusion.

This study examines the impact of varying soil strata on ground surface settlement, focusing on the physical mechanical properties of each layer. The results indicate that hard soil layers significantly outperform soft soil layers and heterogeneous soft–hard soil layers. Specifically, in sections entirely composed of hard rock, tunnel excavation induces the least ground surface settlement. Conversely, in sections entirely composed of soft rock,

tunnel excavation leads to the greatest ground surface settlement. Additionally, the relative magnitude relationship between tunnel crown settlement and tunnel floor uplift varies with changes in the stratum composite ratio.

As illustrated in Figure 10, the smallest surface settlement is observed when constructing a shield tunnel under fully hard rock. This can primarily be attributed to the robust stability of the surrounding rock around the tunnel, which exhibits an effective arching effect that significantly reduces its own deformation [29]. However, as the shield tunneling machine advances, the construction gap at the tail of the shield prompts both the machine and the surrounding soil to descend towards the tunnel's base due to gravity [30]. This action results in an enlargement of the gap in the tunnel's upper section, leading to geological losses. Full-section hard rock, compared to other geological layers, offers superior geological stability and prevents significant over-excavation, thereby substantially reducing such losses [31]. The settlement trough's influence range is directly proportional to the strata's composite ratio; an increase in this ratio will amplify the influence range, albeit with minimal sensitivity. Additionally, it can be inferred from the figure that excavating the right tunnel leads to a certain rise in surface settlement above the left tunnel, a phenomenon correlated with the strata's composite ratio.

The relationship between stratum loss and surface maximum settlement value increases in tandem with the rise in the stratum composite ratio. This correlation is clearly reflected in both the overall settlement trough curve distribution and the surface settlement value, indicating a pronounced sensitivity to changes in surface settlement due to variations in the stratum composite ratio. As depicted in Figure 11, post-excavation, the left-line tunnel exhibits a higher settlement than the right-line tunnel. Notably, the influence of the stratum composite ratio on the ultimate settlement of the left line is not significantly different from its effect on the right-line tunnel's settlement. The observed discrepancy in settlement between the left and right lines, stemming from differing stratum composite ratios, amounts to approximately 0.32 mm. This variation can be attributed to the disruption caused by the excavation of the double-line tunnel. The disturbance induced by the excavation of the left-line tunnel relative to the right-line tunnel is relatively minor. Upon the completion of the left-line tunnel excavation, there is minimal ground surface subsidence corresponding to the axis of the right-line tunnel. Conversely, the disturbance caused by the excavation of the right-line tunnel relative to the left-line tunnel is more pronounced and intensifies with an increase in the stratum composite ratio. Figure 12 illustrates this relationship, depicting the variation in settlement amount of the left-line tunnel as an evaluation index for disturbance size. The figure indicates that, when the stratum composite ratio is 0%, the disturbance value is 5.31 mm. As the stratum composite ratio increases, so does the disturbance value; for instance, when the stratum composite ratio reaches 100%, the disturbance value escalates to 7.03 mm. It is also clear that the stratum composite ratio significantly influences subsequent tunnel excavation disturbances, resulting in a superposition effect of subsidence.

As illustrated in Figure 13, the influence of the preceding left-line tunnel on the central section of the joint line between both tunnels amplifies with an increase in the formation composite ratio. Upon concluding the left-line excavation, settlement values at this juncture under different formation composite ratios are recorded as 3.15 mm, 3.22 mm, 3.38 mm, 3.58 mm, 3.58 mm, 3.86 mm, and 3.97 mm, respectively. The curve displays a relatively gentle slope, implying that the differentiation effect of the formation composite ratio is minimal. However, upon the completion of the right-line excavation, the corresponding settlement value is 5.92 mm, 6.02 mm, 6.41 mm, 6.71 mm, 6.85 mm, 7.36 mm, and 7.61 mm, respectively. At this point, the settlement curve becomes steeper, indicating that the formation composite ratio has a more significant impact on the secondary disturbance caused by subsequent tunnel excavations. The aforementioned pattern of secondary disturbance induced by the right-line tunnel's excavation within the left-line tunnel remains consistent. The disturbance values for different formation composite ratios here are recorded as 2.77 mm, 2.80 mm, 3.02 mm, 3.13 mm, 3.27 mm, 3.50 mm, and 3.64 mm, respectively.

Variations in the stratum composite ratio result in differences in the degree of stratum settlement. Typically, the settlement pattern of the stratum demonstrates high consistency, characterized by settlement at the tunnel crown and uplift at the tunnel base. The sensitivity of the shield tunneling settlement time curve to the stratum composite ratio is relatively low. Hard soil layers perform better than soft soil layers and heterogeneous soft–hard soil layers. Among all sections of hard rock, surface settlement due to tunnel excavation is minimal; however, among all sections of soft rock, it is most pronounced. Concurrently, the relative magnitude relationship between tunnel crown settlement and tunnel base uplift also varies with the stratum composite ratio. The figure illustrates that the stability of the surrounding rock in an excavated tunnel is inversely proportional to the size of the stratum composite ratio. As this ratio increases, the stability of the surrounding rock transitions from strong to weak, leading to a gradual increase in crown settlement. In instances where a left-line tunnel is constructed first, it disrupts the original stress balance state of the soil body, causing disturbances to the stratum soil body. The impact of left-line tunnel excavation on a right-line tunnel is minimal; upon the completion of left-line tunnel excavation, there is negligible surface settlement corresponding to the axis line of the right-line tunnel. Conversely, right-line tunnel excavation causes significant disturbance to a left-line tunnel, with larger stratum composite ratios resulting in greater disturbance. Surface subsidence caused by double-line tunnel excavation exhibits an overlapping effect, leading to increased stratum deformation. This superposition effect is most pronounced in the middle section of the joint line between two tunnels' axial centers, and this disturbance escalates with increasing stratum composite ratio.

5.2. Effect of Soil Bin Pressures on Settlement

As illustrated in Figure 14, as the pressure within the earth bin escalates, there is a corresponding gradual decrease in the displacement of the soil body directly in front of the excavation. This reduction also corresponds to a decrease in the influence range. The settlement range of the excavation face predominantly occurs at the front and upper sections of the rock face. This phenomenon primarily arises from the inherent stability of the hard rock beneath the rock face, which resists collapse deformation [31]. However, when compared to the upper section of the soil body, if the pressure within the earth bin falls below the equilibrium support force, it results in insufficient support force. Consequently, this leads to compression into the tunnel, creating an over-excavation scenario. This increases stratum loss and triggers soil body settlement. As depicted in the figure, with an increase in earth bin pressure from 180 kPa to 200 kPa, there is a significant reduction in surface settlement caused by the excavation face. Additionally, the settlement of the soil body ahead of the excavation face tends to be gentler. If soil pressure continues to rise, the soil body in front of the rock face undergoes squeezing deformation, leading to upward uplift displacement on the surface.

As illustrated in Figure 15, as the shield arrives and the pressure within the earth escalates, there is a gradual decrease in the maximum surface settlement. Concurrently, the pressure within the earth continues to rise, causing the deformation of the surface at the tunnel axis to transition from subsidence to uplift. The surface deformation reaches its minimum when the pressure within the earth is 140 kPa. The width of the settlement groove remains relatively consistent throughout, with its influence range largely confined to approximately 50 m without significant deviation. Consequently, variations in the pressure within the earth exert minimal impact on the width of the lateral settlement groove of the surface.

As illustrated in Figure 16, there is a direct linear relationship between the increase in soil bin pressure and surface deformation as the shield reaches its position. This relationship can be expressed by the function $y = -10.2 + 0.0078x$, derived from the surface deformation data. According to the fitted curve and the law depicted in Figure 15, the minimum surface deformation occurs when the soil bin pressure is set at 130 kPa. Given this numerical simulation condition, it is most prudent to select a soil bin pressure of 130 kPa. If the

pressure exceeds this value, while reducing the risk of ground subsidence, it results in uplift deformation on the ground, which adversely affects buildings and regular production and life activities [32]. In early shield construction stages, an overly small pressure in the soil bin may lead to face instability and subsequent ground subsidence. However, an unguided increase in pressure could lead to counterproductive outcomes. To mitigate this risk, prior to construction, it is essential to thoroughly examine hydrogeological conditions. This should be conducted in conjunction with tunnel burial depth to ensure that the chosen soil bin pressure is reasonable. If necessary, numerical simulations can be employed to further reduce construction risks.

5.3. Effect of Grouting Pressures on Settlement

As depicted in Figure 17, the settlement area in front of the face along the direction of shield tunneling displays a funnel-shaped pattern under different grouting pressures. The quantity of settlement gradually decreases from the top of the arch to the ground surface. However, the range of influence is such that the longitudinal settlement area at the ground surface approximates one tunnel diameter. Importantly, there is no significant difference in the settlement range and numerical value of the strata, indicating that the grouting pressure has minimal impact on the stability of the face. Additionally, the settlement of the strata within the excavated area behind the face remains consistent, suggesting that, under these working conditions, the magnitude of grouting pressure does not significantly affect the longitudinal temporal course of strata changes. As shown in Figure 18, the lateral settlement cloud diagrams for strata perpendicular to the shield tunneling direction show variations under different grouting pressures. Specifically, the maximum settlement of the strata increases from 200 kPa to 400 kPa, while its minimum decreases from 11.53 mm to 10.69 mm. Notably, the peak settlement is observed at the apex of the arch. A comparison of the five lateral settlement cloud diagrams reveals that the settlement range remains consistent from top to bottom, transitioning from broad at the top to narrow at the base. Furthermore, as the grouting pressure increases, the settlement range on the surface decreases, although this change is relatively minor overall.

Figure 19 demonstrates that settlement curves for varying grouting pressures nearly align, with minor differences in grouting pressure resulting in negligible variations in surface settlement. Upon shield arrival, the maximum surface settlement approximates 4.5 mm, whereas after the left-line tunnel traverses, it rises to approximately 10 mm. Greater grouting pressure only induces minimal changes in settlement. It is important to highlight that this numerical model simplifies the grouting body into an equivalent layer and presumes complete slurry filling in building voids by default. It does not account for scenarios where insufficient grouting pressure prevents full slurry filling. Consequently, under these assumptions, the impact of grouting pressure on stratum settlement is deemed relatively insignificant. In essence, the selection criterion for grouting pressure size ensures complete slurry filling in building voids, which also represents the optimal grouting pressure. Exceedingly high grouting pressure does not markedly reduce surface settlement but may introduce other engineering challenges [33]. Therefore, it is imperative to select grouting pressure within a reasonable range.

6. Conclusions

This study utilizes a shield construction section from Qingdao Metro as its foundation, employing numerical simulation methods to investigate the effects of varying stratum composite ratios, grouting pressures, and soil bin pressures on ground surface deformation. The quantity of ground surface deformation is used as the evaluation index to analyze the correlation between various construction parameters and ground surface deformation. The findings of this research are as follows:

(1) Surface settlement depends on stratum composite ratios. Hard rock results in minimal settlement, while soft rock leads to significant settlement. Surrounding rock stability inversely correlates with the stratum composite ratio. As this ratio increases,

stability decreases, causing settlement to gradually rise at the arch's apex. Right-line tunnel excavation disturbs the left-line tunnel more, and this disturbance intensifies with higher stratum composite ratios.

(2) Surface deformation directly correlates with the soil bin pressure. Data fitting yields a linear relationship: $y = -10.2 + 0.0078x$. Settlement range decreases as soil bin pressure rises. Settlement occurs mainly in front and above the soil body. Optimal soil bin pressure is 130 kPa, minimizing surface deformation. Higher pressures cause extrusion deformation, leading to ground uplift.

(3) Grouting pressure has limited impact on stratum settlement over time. Settlement curves remain similar regardless of pressure, indicating minimal differences in surface settlement. This model simplifies grouting as a waiting layer, assuming slurry fills all voids. Thus, the influence of grouting pressure on settlement is minor.

(4) Factors affecting stratum settlement rank as follows: stratum composite ratio > earth pressure > grouting pressure. In coastal tunnels, excavating more hard rock enhances safety. Low soil bin pressure can cause instability and subsidence, while high pressure can lead to uplift. Pre-construction review of hydrogeological conditions and tunnel depth is crucial for choosing appropriate soil bin pressure. Numerical simulations can help mitigate risks. Optimal grouting pressure ensures voids are filled; excessive pressure does not significantly reduce settlement.

(5) Due to the influence of modeling accuracy and computational efficiency, this article does not study the torque of shield tunneling machine cutterhead, and further research will be conducted in this area in the future. The rock mass is currently perceived as intact, with no consideration given to the joint and fissures within it. However, their potential adverse effects on the mass of the mask warrant further investigation in subsequent research.

Author Contributions: Conceptualization, J.X., P.S. and S.W.; methodology, J.X., S.W. and W.Q.; software, X.W., Z.H. and S.S.; data curation, X.Z. and X.C.; writing—original draft preparation, X.W.; writing—review and editing, X.W., P.S., W.Q., X.Z. and Z.H. All authors have read and agreed to the published version of the manuscript.

Funding: The work was partially supported by the Innovation Capability Support Program of Shaanxi (2023-CX-TD-35); the Key Research and Development Program of Shaanxi (2023KXJ-159); the Key Research and Development Projects of Shaanxi Province (2024GX-YBXM-372 and 2024QCY-KXJ-176); and the Department of Transport of Shaanxi Province (22-38K and 23-39R).

Data Availability Statement: All data generated or analyzed during this study are included in this published article.

Conflicts of Interest: The authors declare no conflicts of interest.

References

1. Yang, H.; Shi, H.T.; Jiang, X.L.; Liu, C. Influence of Construction Process of Double-Line Shield Tunnel Crossing Frame Structure on Ground Settlement. *Geotech. Geol. Eng.* **2020**, *38*, 1531–1545. [CrossRef]
2. Wang, F. Evaluation of Surface Subsidence During TBM Construction of Urban Tunnels Based on Generalized Rheological Theory. *Geotech. Geol. Eng.* **2022**, *40*, 1323–1330. [CrossRef]
3. Salour, F.; Erlingsson, S. Permanent deformation characteristics of silty sand subgrades from multistage RLT tests. *Int. J. Pavement Eng.* **2017**, *18*, 236–246. [CrossRef]
4. Akbarimehr, D.; Rahai, A.; Eslami, A.; Karakouzian, M. Deformation Characteristics of Rubber Waste Powder-Clay Mixtures. *Sustainability* **2023**, *15*, 12384. [CrossRef]
5. Peck, R. Deep excavations and tunnelling in soft ground. In Proceedings of the 7th International Conference on Soil Mechanics and Foundation Engineering, Mexico City, Mexico; 1969; pp. 225–290. Available online: https://www.issmge.org/publications/publication/deep-excavations-and-tunneling-in-soft-ground (accessed on 10 April 2024).
6. O'Reilly, M.P.; New, B.M. Settlements above tunnels in the United Kingdom—Their magnitude and prediction. *Proc. Tunn.* **1982**, 173–181. Available online: https://trid.trb.org/view/186714 (accessed on 10 April 2024). [CrossRef]
7. Mair, R.; Taylor, R.; Bracegirdle, A. Subsurface settlement profiles above tunnels in clay. *Geotechnique* **1995**, *45*, 361–362. [CrossRef]
8. Attewell, P.B.; Yeates, J.; Selby, A.R. *Soil Movements Induced by Tunnelling and their Effects on Pipelines and Structures*; Thomson Science and Professional: New York, NY, USA, 1986.
9. Liu, J.; Hou, X. *Shield Tunnel*; China Railway Publishing House: Beijing, China, 1991.

10. Chen, C.; Zhao, C.; Wei, G.; Ding, Z. Prediction of soil settlement induced by double-line shield tunnel based on Peck formula. *Rock. Soil. Mech.* **2014**, *35*, 2212–2218. (In Chinese)
11. Zhang, Y.; Cao, W.; Zhou, S.; Zhou, S.; Xing, J.; Huang, Y. Prediction of three-dimensional subface and subsurface settlement caused by shield tunnelling based on Peck formula. *J. Railw. Sci. Eng.* **2021**, *18*, 153–161. (In Chinese)
12. Zhang, Z.; Zhang, M.; Jiang, Y.; Bai, Q.; Zhao, Q. Analytical prediction for ground movements and liner internal forces induced by shallow tunnels considering non-uniform convergence pattern and ground-liner interaction mechanism. *Soils Found.* **2017**, *57*, 211–226. [CrossRef]
13. Kong, F.C.; Lu, D.C.; Du, X.L.; Shen, C.P. Displacement analytical prediction of shallow tunnel based on unified displacement function under slope boundary. *Int. J. Numer. Anal. Met.* **2019**, *43*, 183–211. [CrossRef]
14. Zeng, B.; Huang, D. Soil deformation induced by Double-O-Tube shield tunneling with rolling based on stochastic medium theory. *Tunn. Undergr. Space Technol.* **2016**, *60*, 165–177. [CrossRef]
15. Rowe, R.; Lee, K. An evaluation of simplified techniques for estimating three-dimensional undrained ground movements due to tunnelling in soft soils. *Can. Geotech. J.* **2011**, *29*, 39–52. [CrossRef]
16. He, C.; Jiang, Y.C.; Fang, Y.; Feng, K.; Wang, J. Impact of Shield Tunneling on Adjacent Pile Foundation in Sandy Cobble Strata. *Adv. Struct. Eng.* **2013**, *16*, 1457–1467. [CrossRef]
17. He, C.; Wang, Y.; Fang, Y.; Xie, J.; Zhao, Q. Similarity model test of Earth-Pressure-Balanced shield tunneling process. *China Civ. Eng. J.* **2012**, *45*, 244–255.
18. Feng, Z.Y.; Liu, B.; Zhang, S.J.; Kang, F.; Hui, H.P.; Tang, Q. Dynamic Failure Process of Soil Particles at the End of Shield Tunnel Based on Discrete Element. *Environ. Sci. Eng.* **2023**, 509–520. [CrossRef] [PubMed]
19. Yang, J.; Xu, D.; Cai, J.; Zhou, Y. Influence of Tunneling on Adjacent Foundations Based on Boundary Element Method. *J. Chongqing Jiaotong Univ. Nat. Sci.* **2019**, *38*, 35–40+122.
20. Lei, H.Y.; Shi, L.; Hu, Y.; Zheng, G.; Zhang, T.Q.; Jia, R. Ground movement and settlement prediction induced by double-track curvature shield tunneling. *Acta Geotech.* **2024**. [CrossRef]
21. Li, S.; Chen, Y.X.; Huang, L.H.; Guo, E.P. Study on Response and Influencing Factors of Shield Single/Twin Tunnel under Seismic Loading using FLAC 3D. *Shock. Vib.* **2022**, *2022*, 2224198. [CrossRef]
22. Yuan, W.; Fu, H.L.; Zhang, J.B.; Huang, Z. Analytical Prediction for Tunneling-Induced Ground Movements with Modified Deformation Pattern. *Int. J. Geomech.* **2018**, *18*, 04018039.1–04018039.12. [CrossRef]
23. Guo, L. Law of Ground Surface Settlement Caused by Shield Tunnel Construction in Sand/Clay Compound Strata. *Mod. Tunn. Technol.* **2017**, *54*, 130–137.
24. Zhou, L.; Zhang, M.; Wang, W.; Lv, Y.; Han, J.; Zhang, J. Analysis of the Influence of Mixed stratum of Up Soft and Down Hard on Shield Tunnel Construction in Guangzhou. *Railw. Stand. Des.* **2018**, *62*, 113–114.
25. Ochmanski, M.; Modoni, G.; Bzówka, J. Numerical analysis of tunnelling with jet-grouted canopy. *Soils Found.* **2015**, *55*, 929–942. [CrossRef]
26. Anato, N.J.; Chen, J.; Tang, A.P.; Assogba, O.C. Numerical Investigation of Ground Settlements Induced by the Construction of Nanjing WeiSanLu Tunnel and Parametric Analysis. *Arab. J. Sci. Eng.* **2021**, *46*, 11223–11239. [CrossRef]
27. Li, X.; Lu, D.; Sun, H.; Hu, J.; Li, J.; Wu, X.; Xu, J. Stratum Deformation Law of Tidal River by Shield Tunneling under Shallow Overburden Soil. *Sci. Technol. Eng.* **2023**, *23*, 1270–1277.
28. Sun, F.X.; Jin, Z.Z.; Wang, C.L.; Gou, C.F.; Li, X.C.; Liu, C.; Yu, Z. Case Study on Tunnel Settlement Calculations during Construction Considering Shield Disturbance. *Ksce J. Civ. Eng.* **2023**, *27*, 2202–2216. [CrossRef]
29. He, J.Z.; Liao, S.M.; Liu, M.B.; Sun, J.C.; Xi, X.G. The soil arching effect induced by shield tunnelling under asymmetric surface loading. *Comput. Geotech.* **2023**, *154*, 105145. [CrossRef]
30. Zhang, Z.G.; Chen, J.; Zhu, Z.G.; Wei, G.; Wu, Z.T.; Chen, Z.K. Analysis of ground settlement induced by small radius curve tunnel excavation considering shield articulation effect. *Rock. Soil. Mech.* **2023**, *44*, 1165–1178. [CrossRef]
31. Ding, J.W.; Zhang, S.; Zhang, H.; Guo, C.; Liao, Z.S.; Liu, H.G. Ground Settlement Caused by Shield Tunneling in Soil-Rock Composite Strata. *J. Perform. Constr. Fac.* **2021**, *35*, 04021057.1–04021057.12. [CrossRef]
32. Chen, R.P.; Meng, F.Y.; Ye, Y.H.; Liu, Y. Numerical simulation of the uplift behavior of shield tunnel during construction stage. *Soils Found.* **2018**, *58*, 370–381. [CrossRef]
33. Zhong, X.C.; Huang, S.Y.; Hum, R.G.; Zhu, C.; Hu, Y.K.; Chen, X.Q. Longitudinal uplift characteristics of segments of shield tunnels based on buoyancy of grouting. *Rock. Soil. Mech.* **2023**, *44*, 1615–1624. [CrossRef]

Disclaimer/Publisher's Note: The statements, opinions and data contained in all publications are solely those of the individual author(s) and contributor(s) and not of MDPI and/or the editor(s). MDPI and/or the editor(s) disclaim responsibility for any injury to people or property resulting from any ideas, methods, instructions or products referred to in the content.